Catalytic activation via π–backbonding in halogen bonds

Andrew Wang[a,†] and Pierre Kennepohl[*a,b]

a. Department of Chemistry, The University of British Columbia, 2036 Main Mall, Vancouver, British Columbia, Canada.

b. Department of Chemistry, University of Calgary, 2500 University Drive NW, Calgary, Alberta, Canada.

ABSTRACT: The role of halogen bonding (XB) in chemical catalysis has largely involved using XB donors as Lewis acid activators to modulate the reactivity of partner Lewis bases. We explore a more uncommon scenario, where a Lewis base modulates reactivity via a spectator halogen bond interaction. Our computational studies reveal that spectator halogen bonds may play an important role in modulating the rate of S_N2 reactions. Most notably, π acceptors such as PF_3 significantly decrease the barrier to substitution by decreasing electron density in the very electron rich transition state. Such π-backbonding represents an example of a heretofor unexplored situation in halogen bonding: the combination of both σ-donation and π-backdonation in this "non-covalent" interaction. The broader implications of this observation are discussed.

Introduction

Applications of halogen bonding and other forms of secondary interactions[1] have increased dramatically in the last decade.[2] The reversible, yet highly directional, halogen bond (XB) has been used successfully in crystal engineering,[3–5] supramolecular chemistry,[6,7] selective binding and sensing[8–11], and medicinal chemistry.[12] More recently, they have been applied towards chemical catalysis.[13–15] Many examples of XB activation for chemical processes have focused on developing highly electron-deficient *XB* donors[A] (the electron acceptor, i.e. the Lewis acid A-X, Figure 1) that modulate the reactivity of *XB acceptors* (the electron donor, i.e., the Lewis base D). In such cases, the catalyst acts as a classical Lewis acid catalyst. Examples of Lewis base catalysis where an A-X moiety acts as the target for activation are rare. To our knowledge, literature examples are limited to stoichiometric activation, such as those demonstrated in perfluoroalkylation reactions.[13,16,17]

XBs have typically been described to involve a σ-type electrostatic interaction due to the presence of a zone of electron deficiency at the apex of a terminal halogen atom, termed the σ-hole. The region of positive electrostatic potential leads to an attractive force between the halogen and electron-rich molecules, i.e. good Lewis bases. However, the exact nature of such XB interactions has led to significant debate in the literature. Valence electronic absorption and X-ray absorption spectroscopy have been interpreted within the context of molecular orbital (MO) representations of bonding and, within this framework, reveal strong covalent contributions in many

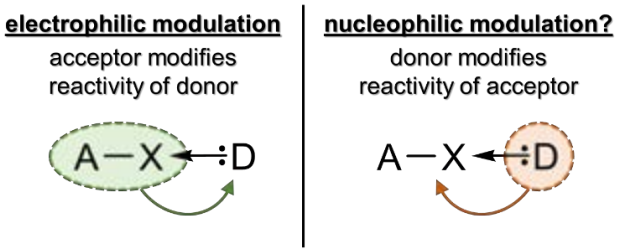

Figure 1. Simplified view of different modes of activation in XB-assisted catalysis. On the left, we depict electrophilic modulation (the most common motif in the literature), where the acceptor (A-X) is the catalyst, which modulates the reactivity of the donor (D). The opposite strategy involves using a catalytic donor (D) to modulate the reactivity of the acceptor (A-X).[A]

halogen bonds.[18–21] For this reason, we have argued that XBs are more analogous to coordination bonds than to the typically-used analogy to hydrogen bonds.[22] It has been argued that covalency (or charge transfer) models relying on MO descriptions are indistinguishable from charge polarization phenomena, and thus focusing on such aspects of chemical bonding are counterproductive.[23–27] Practically, quantifying charge redistribution has been shown to be a powerful approach for the interpretation of chemical phenomena,[28–30] and that describing XB interactions using charge transfer/covalency – especially within the context of chemical reactivity– is both appropriate and useful.[31] One major benefit of the MO formalism is

Scheme 1. Thermodynamic scheme for the symmetric self-exchange S_N2 reaction in the absence (top) and presence (bottom) of XB donor-acceptor interactions. Energies calculated include both enthalpies (E = H) and free energies (E = G). A series of different substitution patterns (R_1, R_2) were chosen to take account of other possible electronic contributions (Note 2 for details). Four different donors were used in this study: NH_3, CO, PF_3, and PH_3.

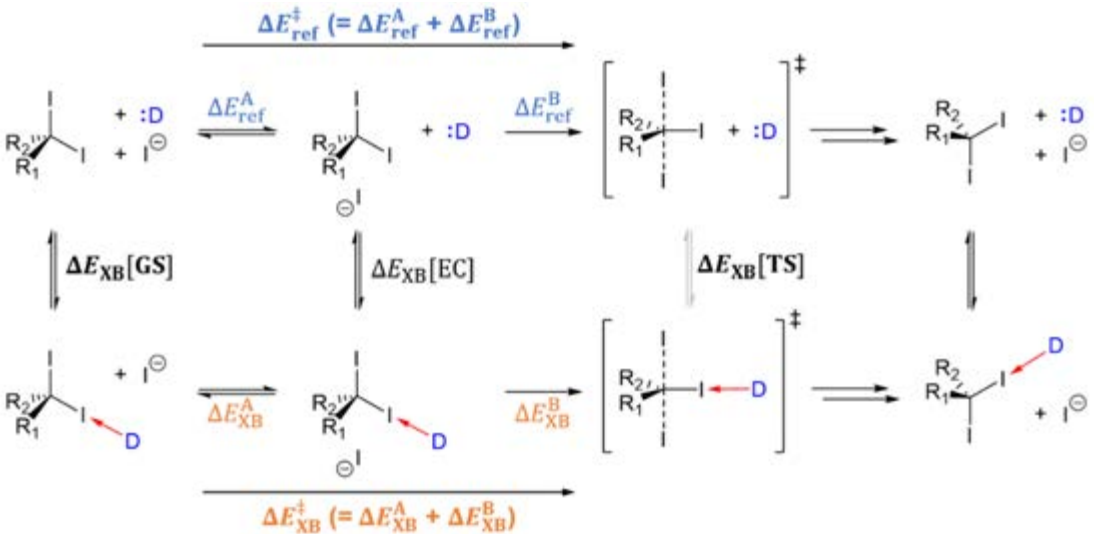

the convenience and power of differentiating between different types of donor/acceptor interactions, *i.e.*, separating σ/π/δ-type bonding contributions. Notably, π-type bonding in XB interactions was recently observed both computationally[32,33, [B]] and experimentally.[33] This discovery implies that XB interactions may be quite complex and could be tunable to achieve specific objectives.

Systems which display nucleophilic modulation of the reactivity of a moiety A-X via halogen bonding (Figure 1) are quite rare, which initially perplexed us until we observed that XB formation should *inhibit* A-X bond cleavage via stabilization of the reactants (*vide infra*). Dampening of the reactivity of the A-X moiety allows for the possibility of using the A-X to modulate other aspects of A. We employ density functional theory (DFT) calculations to explore one such case: the symmetric nucleophilic self-exchange of geminal diiodomethanes ($I^- + R_2CI_2 \rightleftharpoons R_2CI_2 + I^-$). We find that XB interactions invariably deactivates that iodo group towards substitution, thus potentially allowing for an indirect catalytic influence of XB on another group.

We chose to explore symmetric self-exchange S_N2 reactions to simplify the overall process (Scheme 1). Geminal diiodomethanes allow for one spectator iodine to be involved in XB throughout the reaction and one reactive iodine. Using a range of substituents with differing electronic properties (R_1/R_2 = H, CH_3, CN, @Cy[C]) helps us establish general trends in behaviour across a wide range of potential substrates.

These studies have uncovered the importance of π-backbonding as a mechanism for catalyzing substitution by decreasing Pauli repulsion in the transition state. We observe that prototypical σ-donor Lewis bases such as amines both directly and indirectly inhibit S_N2 reactivity, yet a σ-donor + π-acceptor such as PF_3 can significantly lower the activation barrier for substitution. The mechanism of activation relies on a substantial decrease in Pauli repulsion in the transition state.[34,35] Charge decomposition analysis confirms the critical role of XB π-backbonding in lowering the activation barrier and enhancing reaction rates.

Results and Discussion

Symmetric self-exchange S_N2 reactions often have a double well reaction profile, which includes both the formation of the encounter complex and substitution itself (Scheme 1). Energies for species in the ground state (GS), encounter complex (EC), and at the transition state (TS) were calculated. As expected, the enthalpy of stabilization due to halogen bonding (ΔH^o_{XB}) is typically negative due to a favourable donor-acceptor interaction, whereas ΔG^o_{XB} is positive due to entropy.[6] We focus our attention on enthalpic contributions in this analysis due to our interest in the role of electronic contributions to the observed processes. With regards to the activation barriers, we find that Gibbs free energy results ($\Delta\Delta G^‡$) yield similar trends to $\Delta\Delta H^‡$ as shown in Figure S1.

We define the reaction barrier from separated reactants to the transition state (see Figure 1).[36] This simplifies our analysis and allows us to avoid some of the specific complexities related to the encounter complex itself.[37] The effect of halogen bonding in the ground state is particular easy to quantify and thus provides a convenient reference point. The effect of spectator XB interactions on the reaction barrier are defined as the difference between the enthalpy of activation in the presence of XB ($\Delta H^‡_{XB}$) and the enthalpy of activation without XB ($\Delta H^‡_{ref}$) such that $\Delta\Delta H^‡ = \Delta H^‡_{XB} - \Delta H^‡_{ref}$. $\Delta\Delta H^‡$ may also be expressed as the difference between the XB stabilization of the GS (ΔH^o_{XB}[GS]) and that of the TS (ΔH^o_{XB}[TS]), *i.e.*, $\Delta\Delta H^‡ = \Delta H^o_{XB}[TS] - \Delta H^o_{XB}[GS]$, which allows us to consider three regimes depending on the value of $\Delta\Delta H^‡$:

(A) $\Delta\Delta H^{\ddagger} > 0$, *i.e.* $|\Delta H^{o}_{XB}[TS]| > |\Delta H^{o}_{XB}[GS]|$

(B) $\Delta\Delta H^{\ddagger} \approx 0$, *i.e.* $|\Delta H^{o}_{XB}[TS]| \approx |\Delta H^{o}_{XB}[GS]|$

(C) $\Delta\Delta H^{\ddagger} > 0$, *i.e.* $|\Delta H^{o}_{XB}[TS]| < |\Delta H^{o}_{XB}[GS]|$

Importantly, the XB interaction to a particular C-I bond *deactivates* that halogen for substitution. Although the C-I bond is weakened through halogen bonding, the important effect is stabilization of the ground state and loss of the XB interaction in the transition state across a wide range of donors (See Section 5 of the SI). However, if substitution of the other iodine occurs, the effect of halogen bonding differs markedly depending on the nature of the donor.

Figure 2 illustrates the influence of secondary XB interactions on $\Delta\Delta H^{\ddagger}$ as plots of $\Delta H^{\ddagger}_{XB}$ vs. $\Delta H^{\ddagger}_{ref}$. The dashed line corresponds to the situation where $\Delta H^{\ddagger}_{XB} = \Delta H^{\ddagger}_{ref}$; data above that line represent $\Delta\Delta H^{\ddagger} > 0$ and those below the line $\Delta\Delta H^{\ddagger} < 0$. With carbon monoxide as the donor, we observe essentially no effect whatsoever on the predicted barrier for substitution; the entire series of geminal diiodomethanes fall along the reference line such that $\Delta\Delta H^{\ddagger} \approx 0$. For a stronger donor, such as NH_3, the data fall in the regime where $\Delta\Delta H^{\ddagger} > 0$, and thus the XB interaction has a deleterious influence on the kinetics of substitution.[D] These data are similar to what is observed for primary halogen bonds: reaction rates are substantively decreased due to reactant stabilization. By contrast, PF_3 has the opposite effect ($\Delta\Delta H^{\ddagger} < 0$) and is predicted to accelerate substitution. The effect is quite pronounced with an average stabilization of ~10 kJ/mol), and is also observed using $\Delta\Delta G^{\ddagger}$ (see Figure S1). PF_3 has very little effect via a primary XB interaction. The dramatically different behaviour of NH_3 and PF_3 donors in their influence on the substitution reaction required further scrutiny.

Below, we evaluate differences in both the ground state and transition state halogen bonding in each of these cases to identify the origin of this effect.

XB in the ground state. We employed the natural bond orbital (NBO) formalism to evaluate contributions to the XB interactions. Correlation plots between ground state thermodynamic data and σ-type halogen bonding contributions (via 2nd order perturbation analysis of the $D_{\text{lone pair}} \rightarrow \sigma^{*}_{C-I[XB]}$ interaction[E]; $E^{(2)}[\sigma^{*}]$) are shown in Figure S2 (top). For both CO and NH_3, a good correlation is obtained between the strength of σ donation and the overall stabilization obtained via halogen bonding ($\Delta H^{o}_{XB}[GS]$). For PF_3 we find that while the electron donor forms an adduct with the diiodomethane, the XB interaction is very weak. The calculated P-I bond distances are very close to the sum of their Van der Waals radii, thus PF_3 is acting as a very poor donor in the ground state.[6]

XB in the transition state. Correlation plots for the transition states (Figure S2, bottom) differ from the ground state behaviour. In all cases, $\Delta H^{o}_{XB}[TS] < 0$. Correlations are observed with $E^{(2)}[\sigma^{*}]$ for CO and NH_3, yet PF_3 shows no correlation with $E^{(2)}[\sigma^{*}]$ even though thermodynamic stabilization from halogen bonding is now significant (~10 kJ/mol). The XB interaction for PF_3 is thus dominated by some other factor and cannot be fully explained via σ-type bonding.

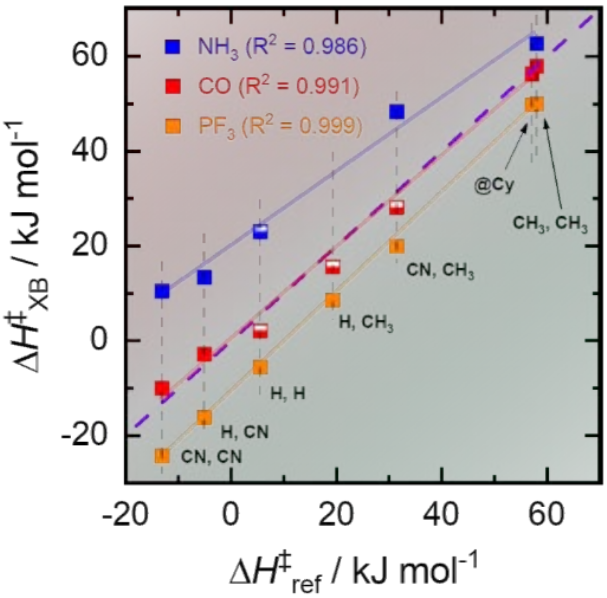

Figure 2. $\Delta H^{\ddagger}_{XB}$ vs. $\Delta H^{\ddagger}_{ref}$ with PF_3 (orange), CO (red), and NH_3 (blue) as the electron donor. The purple dashed line serves as a reference for $\Delta H^{\ddagger}_{XB} = \Delta H^{\ddagger}_{ref}$. Data above the line implies $\Delta H^{\ddagger}_{XB} > \Delta H^{\ddagger}_{ref}$ such that $\Delta\Delta H^{\ddagger} > 0$, and data below the line implies $\Delta H^{\ddagger}_{XB} < \Delta H^{\ddagger}_{ref}$ such that $\Delta\Delta H^{\ddagger} < 0$, with the vertical distance from each data point to the purple dashed line representing the absolute value of $\Delta\Delta H^{\ddagger}$. The sets of substituents are in the form (R_1, R_2). Half-filled squares for CO indicate the presence of additional (small) imaginary frequencies in the TS, and for NH_3 a small imaginary frequency in the ground state (see Tables S6 and S9). (H, CH_3) and (@Cy) not plotted for NH_3 as no XB is present in the TS for those cases. See Figure S1 for $\Delta G^{\ddagger}$.

The influence of these different XB interactions extends to the geometries of the calculated TS structures. Whereas only minor changes are observed for CO as a donor, the effects are both pronounced and divergent when comparing NH_3 and PF_3. The amine donor leads to an overall expansion of the TS, i.e., the bond distances between the electrophilic carbon and the terminal iodides are more elongated in the presence of the spectator halogen bond (Figure S2b). Conversely, the presence of the phosphine leads to contraction of the TS, *i.e.,* these same bonds *are shorter* when the donor is PF_3 (see Figure S2a). This effect correlates with calculated changes in charge distribution within the TS structure. As expected, the amine donor increases electron density at the acceptor via $D \rightarrow \sigma^{*}_{C-I[XB]}$ donation, leading to increased Pauli repulsion in the acceptor. However, the opposite effect is seen with PF_3 which causes charge depletion in the acceptor, which decreases Pauli repulsion.

Natural population analysis (NPA)[38] in the presence/absence of XB interactions (see SI Section 1) allows us to evaluate charge redistribution in the transition state as a result of halogen bonding. These effects are summarized in Scheme 2. For NH_3, halogen bonding results is in significant transfer of charge from the donor to the terminal iodines. For CO, there is a balanced effect where we find very little net change in NPA charges. In the case of PF3, we observe a decrease in electron density at the two terminal iodides, with a concomitant

increase in the perpendicular "C-I···PF_3" fragment. In all cases, the effect of other substituents is minor. These results are generally consistent with the known behaviour of PF_3 in transition metal chemistry, where it is known as an effective π-acceptor ligand.[39]

Scheme 2. Schematic representation of charge flow in each of the transition state structures.

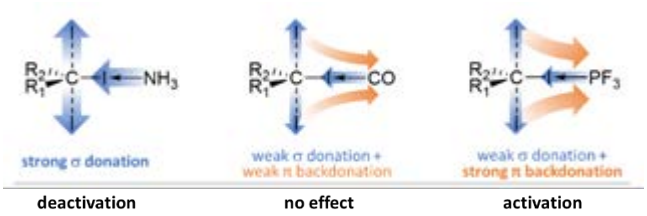

The canonical molecular orbitals in the XB-assisted transition state support the interpretation that π-backbonding plays an important role in stabilizing the transition state. It has previously been noted that three-centre four-electron interaction that defines the S_N2 transition state are of appropriate symmetry to be affected via π-type interactions.[40] Inherently, the second iodo substituent is expected to destabilize the transition state via Pauli repulsion from its filled 5p valence orbitals. However, binding to the π-acidic phosphine in the appropriate orientation provides a pathway to funnel excess electron density away from the I-C-I core, decrease repulsion, and stabilize the transition state via a π-type pathway.

The delocalization can be observed in certain filled molecular orbitals that allow for electron redistribution via π-type interactions. Three of these result in direct electron redistribution from the terminal iodo substituents to PF_3 (I, II, IV in Figure 3). A second pathway is available perpendicular to the CI_3 plane (III in Figure 3). Each of these orbitals is stabilized due to the presence of the XB interactions far more greatly than other orbitals, which are more indirectly influenced by the addition of PF_3 (Figures S17 – S23). These influences are the largest contributions to a global shift in the frontier total density of states of the TS depending on the donor (TDOS, Figure 3b and S25): the amine donor destabilizes the frontier orbitals through charge donation into an already electron rich system, whereas the phosphine donor lowers the TDOS envelope through the π-type pathways described previously.

Charge decomposition analysis (CDA)[41,42] of the contributing pathways provides additional support for the charge flow model outlined in Scheme 2. The contributions from all π-type orbitals identified previously can be broken down as the sum of π-donor ($PF_3 \rightarrow TS$, $\Sigma\rho_\pi^D$, +ve values) and π-acceptor ($PF_3 \leftarrow TS$, $\Sigma\rho_\pi^A$, -ve values) contributions. The data confirm that the influence of PF_3 in the transition state is strongly affected by π-backbonding, with the greatest contributions being made via direct overlap between the in-plane π-type acceptor orbital of the phosphine with filled non-bonding orbitals on the terminal iodo groups mediated by spectator iodo group (Table S19). We also observe a good correlation between the calculated π-backbonding and transition state stabilization across the series (Figure 3c). Overall, CDA confirms that the phosphine participates both via σ-donation and π-backdonation in a manner similar to that which is observed in transition metal complexes[28] and suggests that one may use knowledge from ligand properties in TM chemistry as a guide for defining the influence of these species in halogen-bonded systems. A more complete analysis of both NPA and CDA results are provided in Sections 1 – 4 of the SI.

Table 1. CDA results quantifying charge donation from PF_3 to the diiodomethane substrate in the transition state via σ and π pathways ($\Sigma\rho_\sigma^D$ & $\Sigma\rho_\pi^D$) as well as for π -backdonation ($\Sigma\rho_\pi^A$). Values are listed in $me^- = 10^{-3}e^-$ and rounded to the nearest $0.1me^-$. Expanded versions can be found in Section 4.5 of the SI.

(R_1, R_2)	$\Sigma\rho_\sigma^D$	$\Sigma\rho_\pi^D$	$\Sigma\rho_\pi^A$
CN, CN	+ 27.0	+ 0.1	− 10.4
H, H	+ 13.4	< + 0.1	− 9.4
H, CN	+ 18.3	< + 0.1	− 9.4
CN, CH_3	+ 11.9	< + 0.1	−9.5
H, CH_3	+ 18.3	< + 0.1	− 8.6
CH_3, CH_3	+ 19.3	< + 0.1	− 7.0
@Cy	+ 18.3	< + 0.1	− 6.2

To further probe the importance of π-backbonding in the XB interaction with phosphines, we evaluated the effect of using PH_3, with very poor π-acceptor characteristics compared to PF_3.[39] In all cases but one, XB interactions in the TS could not be identified.[F]

This systematic study clearly demonstrates that very different behaviour can be obtained depending on the electronic nature of the donor used to modulate the substitution reaction. The typically dominant σ-donor properties of a modulator will increase the barrier to substitution by destabilizing the transition state via increased Pauli repulsion. However, good π-acceptor character can overcome this issue and lower the barrier by stabilizing the transition state. Although σ-donor contributions may be stronger overall, π-acceptor character is more efficient in the situation described herein, as it provides a pathway for direct charge redistribution from the very electron rich terminal iodides. Importantly, the inherent ability of halogen bonds to support both σ- and π-type interactions opens the door towards more complex interactions that can be exploited in catalysis.

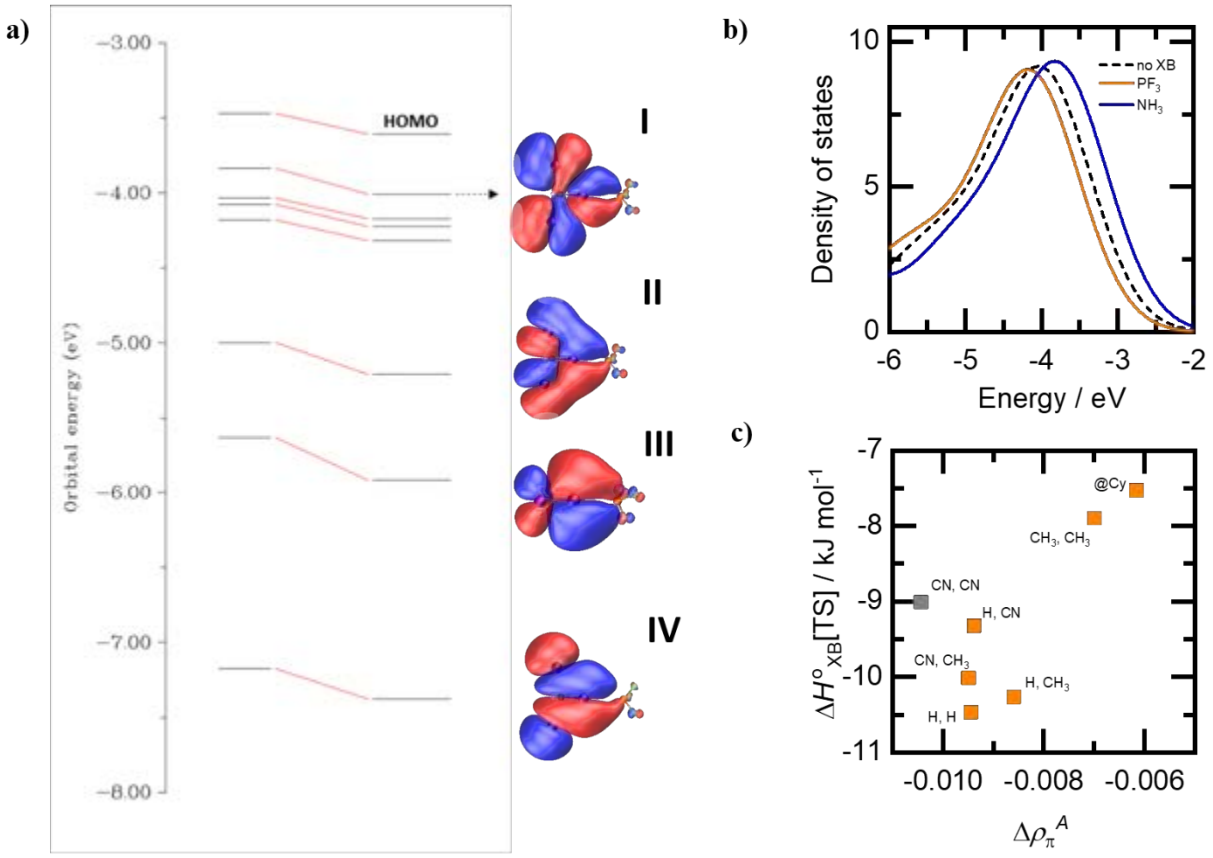

Figure 3. a) MO diagram (using (R_1, R_2) = (H, H) as a representative example) illustrating the decrease in energies of the π-type MOs on the diiodomethane upon complexation with PF_3. The four π-type MOs involved in π-backbonding are shown beside their respective energy levels (the second one from the bottom is orthogonal to the other three). See Figures S17 – S23 for the entire set of substituents and a comparison with NH_3 as the donor. **b)** Gaussian-broadened TDOS around the highest occupied MO (HOMO) for the (R_1, R_2) = (H, H) with no XB (dashed line), PF_3 as the electron donor (orange line), and NH_3 as the electron donor (blue line). See Figure S25 for all substituents. **c)** A plot of ΔH^{o}_{XB}[TS] vs. $\Delta\rho^{A}_{\pi}$ illustrates that π-backdonation contributes to the overall XB stabilization in the TS.

Conclusions

This systematic study of a prototypical S_N2 reaction illustrates the potential role of specific orbital interactions in influencing reactivity via halogen bonds. The combined effect of σ-donation and π-backdonation by PF_3 has a pronounced effect on the predicted rates of substitution through stabilization of the transition state. The π-backbonding is observed to be more efficient in influencing the stability of the transition state via decreased Pauli repulsion. These observations suggest that explicit consideration of both σ- and π-contributions may be more generally required when evaluating the influence of halogen bonding. This strengthens our contention that halogen bonds should be considered in a manner akin to transition metal coordination bonds,[22,33] with electronic interactions of different symmetry playing different roles depending on the inherent electronic nature of the donor/acceptor pair. We demonstrate one example where this behaviour can be used to modulate reactivity and suggest that rational design of halogen bonding catalysts – with appropriate inclusion of π contributions – should be explored.

Computational Methods

Geometry optimization and thermochemistry: All calculations were performed using the Gaussian 09 software (G09)[43] with molecules built in WebMO.[44] The M06-2X functional[45] was used for all calculations owing to its excellent performance on describing thermochemical kinetics and intermolecular interactions,[45,46] and the aug-cc-pVDZ-PP basis set (parameters obtained from the ESML basis set exchange[47,48]) was used for iodine and jun-cc-pVDZ[49] for all other elements. All calculations were performed in the gas phase, at 298.15 K, and 1 atm using an ultrafine integration grid (99 radial shells, 590 angular points).

Ground state structures were optimized to a minimum from a starting distance of ~3 Å between the donor and acceptor atoms and an initial XB angle of ~180 degrees, then followed by frequency calculations for the thermochemical data (calculated from the electronic energies (Section 4 of SI) according to ref. [50]) and to verify the absence of imaginary frequencies.

Transition state calculations were first performed without XB, with an initial search for the transition state via a relaxed potential energy

surface scan along the reaction coordinate (distance between the incoming iodide and the electrophilic carbon), then optimized with the Berny algorithm.[51–55] The QST2 algorithm[56] was used when the Berny algorithm fails to produce an accurate transition state structure. Frequency calculations are then carried out for the thermochemical data and to verify the presence of exactly one imaginary frequency with the vibrational mode corresponding to substitution of LG by Nu along the reaction coordinate. Transition state structures with XB were optimized from an initial configuration consisting of the optimized TS of the geminal iodide and the electron donor placed at a distance of ~ 3 Å between the donor and acceptor atoms and an initial XB angle of ~180 degrees, followed by the same procedure for optimizing the TS without XB.

Generalizing the XB stabilization energies in the GS and TS to being any thermodynamic quantity E (for this study $E = H$ or $E = G$), the XB stabilization (ΔE_{XB}) is calculated as follows:

$$\Delta E_{\mathrm{XB}} = E_{\mathrm{complex}} - (E_{\mathrm{diiodomethane}} + E_{\mathrm{electron\ donor}})$$

where $E_{\mathrm{diiodomethane}}$ and $E_{\mathrm{electron\ donor}}$ refer to the corresponding isolated species. Because of the nature of the square scheme involved in this study (Scheme 1), it follows from conservation of energy that

$$\Delta\Delta E^{\ddagger} = \Delta E^{\ddagger}_{\mathrm{XB}} - \Delta E^{\ddagger}_{\mathrm{ref}} = \Delta E_{\mathrm{XB}}[\mathrm{TS}] - \Delta E_{\mathrm{XB}}[\mathrm{GS}]$$

($E_{\mathrm{electron\ donor}}$ cancels out in the derivation).

Single point calculations, MO analysis, TDOS, CDA, and NBO/NPA: Single point calculations were performed using G09 with both M06-2X/jun-cc-pVDZ (aug-cc-pVDZ-PP for iodine) and M06-2X/def2-TZVP. The results of MO analysis from the def2-TZVP and jun/aug-cc-pVDZ basis sets were qualitatively similar for the entire series of diiodomethanes, so the former was used for NBO calculations and density of states. For MO plotting (diagrams/figures) and CDA, M06-2X/def2-TZVP was used.

NBO and NPA calculations were carried out with the NBO package built into G09. MO energy diagrams, CDA, and Gaussian-broadened density of states (calculated via the Hirshfield method) were obtained using Multiwfn.[57] MO cube files (~512 000 grid points) were generated using Multiwfn, rendered using the Visual Molecular Dynamics software, [58] and traced with POV-Ray 3.6.[59]

ASSOCIATED CONTENT

Supporting Information is available free of charge at http://pubs.acs.org/[doi info].

AUTHOR INFORMATION

Corresponding Author

pierre.kennepohl@ucalgary.ca

Present Addresses

† Department of Chemistry, University of Toronto, 80 St. George Street, Toronto, Ontario, Canada

Author Contributions

The manuscript was written through contributions of all authors. / All authors have given approval to the final version of the manuscript. / ‡These authors contributed equally. (match statement to author names with a symbol)

Funding Sources

Any funds used to support the research of the manuscript should be placed here (per journal style).

Notes

A. There is some potential for confusion due to the formal definition of halogen bonds where the XB donor is formally the Lewis acid (electron acceptor), and the XB acceptor is the Lewis acid (electron donor). We prefer to align our nomenclature with that used in transition metal chemistry where donor/acceptor character refers to electron density.

B. There are also reports of σ-type XB interactions between a π electron cloud with electron-deficient halogens called "halogen-π interactions" but these are very different from π-type contributions a halogen bonds.

C. We adopt the shorthand (R_1, R_2) in the text to describe the substituents on each diiodomethane. R_1 and R_2 involve all combinations of H, CH_3, and CN, and @Cy refers to a cyclohexane ring, taking up the positions of R_1 and R_2, with the electrophilic carbon as part of the ring.

D. For NH_3 with the sets of substituents (H, CH_3) and (@Cy), we were unable to obtain a TS structure with XB.

E. I[XB] refers to the iodine directly involved in XB.

F. For all substituents in the series except (@Cy), where $\Delta H^{o}_{\mathrm{XB}}[\mathrm{TS}] \approx$ -4 kJ/mol, there was either no XB or convergence could not be achieved.

The authors declare no conflicts of interests.

ACKNOWLEDGMENT

The authors would like to thank UBC Chemistry, WestGrid, and Compute Canada for computational resources used for this work.

REFERENCES

(1) Crabtree, R. H. Hypervalency, Secondary Bonding and Hydrogen Bonding: Siblings under the Skin. *Chem. Soc. Rev.* **2017**, *46* (6), 1720–1729. https://doi.org/10.1039/C6CS00688D.

(2) Cavallo, G.; Metrangolo, P.; Milani, R.; Pilati, T.; Priimagi, A.; Resnati, G.; Terraneo, G. The Halogen Bond. *Chem. Rev.* **2016**, *116* (4), 2478–2601. https://doi.org/10.1021/acs.chemrev.5b00484.

(3) Mukherjee, A.; Tothadi, S.; Desiraju, G. R. Halogen Bonds in Crystal Engineering: Like Hydrogen Bonds yet Different. *Acc. Chem. Res.* **2014**, *47* (8), 2514–2524. https://doi.org/10.1021/ar5001555.

(4) Teyssandier, J.; Mali, K. S.; De Feyter, S. Halogen Bonding in Two-Dimensional Crystal Engineering. *ChemistryOpen* **2020**, *9* (2), 225–241. https://doi.org/10.1002/open.201900337.

(5) Ateş, Ö. D.; Zorlu, Y.; Kanmazalp, S. D.; Chumakov, Y.; Gürek, A. G.; Ayhan, M. M. Halogen Bonding Driven Crystal Engineering of Iodophthalonitrile Derivatives. *CrystEngComm* **2018**, *20* (27), 3858–3867. https://doi.org/10.1039/C8CE00594J.

(6) Gilday, L. C.; Robinson, S. W.; Barendt, T. A.; Langton, M. J.; Mullaney, B. R.; Beer, P. D. Halogen Bonding in Supramolecular Chemistry. *Chem. Rev.* **2015**, *115* (15), 7118–7195. https://doi.org/10.1021/cr500674c.

(7) Metrangolo, P.; Meyer, F.; Pilati, T.; Resnati, G.; Terraneo, G. Halogen Bonding in Supramolecular Chemistry. *Angew. Chem. Int. Ed.* **2008**, *47* (33), 6114–6127. https://doi.org/10.1002/anie.200800128.

(8) Langton, M. J.; Robinson, S. W.; Marques, I.; Félix, V.; Beer, P. D. Halogen Bonding in Water Results in Enhanced Anion Recognition in Acyclic and Rotaxane Hosts. *Nat. Chem.* **2014**, *6* (12), 1039–1043. https://doi.org/10.1038/nchem.2111.

(9) Lim, J. Y. C.; Bunchuay, T.; Beer, P. D. Strong and Selective Halide Anion Binding by Neutral Halogen-Bonding [2]Rotaxanes in Wet Organic Solvents. *Chem. Eur. J.* **2017**, *23* (19), 4700–4707. https://doi.org/10.1002/chem.201700030.

(10) Mullaney, B. R.; Thompson, A. L.; Beer, P. D. An All-Halogen Bonding Rotaxane for Selective Sensing of Halides in Aqueous Media. *Angew. Chem. Int. Ed.* **2014**, *53* (43), 11458–11462. https://doi.org/10.1002/anie.201403659.

(11) Hein, R.; Borissov, A.; Smith, M. D.; Beer, P. D.; Davis, J. J. A Halogen-Bonding Foldamer Molecular Film for Selective Reagentless Anion Sensing in Water. *Chem. Commun.* **2019**, *55* (33), 4849–4852. https://doi.org/10.1039/C9CC00335E.

(12) Wilcken, R.; Zimmermann, M. O.; Lange, A.; Joerger, A. C.; Boeckler, F. M. Principles and Applications of Halogen Bonding in Medicinal Chemistry and Chemical Biology. *J. Med. Chem.* **2013**, *56* (4), 1363–1388. https://doi.org/10.1021/jm3012068.

(13) Sutar, R. L.; Huber, S. M. Catalysis of Organic Reactions through Halogen Bonding. *ACS Catal.* **2019**, *9* (10), 9622–9639. https://doi.org/10.1021/acscatal.9b02894.

(14) Kuwano, S.; Suzuki, T.; Yamanaka, M.; Tsutsumi, R.; Arai, T. Catalysis Based on C–I···π Halogen Bonds: Electrophilic Activation of 2-Alkenylindoles by Cationic Halogen-Bond Donors for [4+2] Cycloadditions. *Angew. Chem. Int. Ed.* **2019**, *58* (30), 10220–10224. https://doi.org/10.1002/anie.201904689.

(15) Bulfield, D.; Huber, S. M. Halogen Bonding in Organic Synthesis and Organocatalysis. *Chem. Eur. J.* **2016**, *22* (41), 14434–14450. https://doi.org/10.1002/chem.201601844.

(16) Beniazza, R.; Remisse, L.; Jardel, D.; Lastécouères, D.; Vincent, J.-M. Light-Mediated Iodoperfluoroalkylation of Alkenes/Alkynes Catalyzed by Chloride Ions: Role of Halogen Bonding. *Chem. Commun.* **2018**, *54* (54), 7451–7454. https://doi.org/10.1039/C8CC02765J.

(17) Sladojevich, F.; McNeill, E.; Börgel, J.; Zheng, S.-L.; Ritter, T. Condensed-Phase, Halogen-Bonded CF_3I and C_2F_5I Adducts for Perfluoroalkylation Reactions. *Angew. Chem. Int. Ed.* **2015**, *54* (12), 3712–3716. https://doi.org/10.1002/anie.201410954.

(18) Rosokha, S. V.; Stern, C. L.; Ritzert, J. T. Experimental and Computational Probes of the Nature of Halogen Bonding: Complexes of Bromine-Containing Molecules with Bromide Anions. *Chem. Eur. J.* **2013**, *19* (27), 8774–8788. https://doi.org/10.1002/chem.201300577.

(19) Rosokha, S. V.; Vinakos, M. K. Halogen Bond-Assisted Electron Transfer Reactions of Aliphatic Bromosubstituted Electrophiles. *Phys. Chem. Chem. Phys.* **2014**, *16* (5), 1809–1813. https://doi.org/10.1039/C3CP54004A.

(20) Rosokha, S. V. Electron-Transfer Reactions of Halogenated Electrophiles: A Different Look into the Nature of Halogen Bonding. *Faraday Discuss.* **2017**, *203*, 315–332. https://doi.org/10.1039/C7FD00074J.

(21) Robinson, S. W.; Mustoe, C. L.; White, N. G.; Brown, A.; Thompson, A. L.; Kennepohl, P.; Beer, P. D. Evidence for Halogen Bond Covalency in Acyclic and Interlocked Halogen-Bonding Receptor Anion Recognition. *J. Am. Chem. Soc.* **2015**, *137* (1), 499–507. https://doi.org/10.1021/ja511648d.

(22) Mustoe, C. L.; Yu, D.; Gunabalasingam, M.; Patrick, B. O.; Kennepohl, P. Probing Covalency in Halogen Bonds through Donor K-Edge X-Ray Absorption Spectroscopy: Polyhalides as Coordination Complexes. *Faraday Discuss.* **2017**, *203*, 79–91. https://doi.org/10.1039/C7FD00076F.

(23) Clark, T. Halogen Bonds and σ-Holes. *Faraday Discuss.* **2017**, *203*, 9–27. https://doi.org/10.1039/C7FD00058H.

(24) Clark, T.; Murray, J. S.; Politzer, P. Role of Polarization in Halogen Bonds. *Aust. J. Chem.* **2014**, *67* (3), 451. https://doi.org/10.1071/CH13531.

(25) Politzer, P.; Murray, J. S.; Clark, T. Mathematical Modeling and Physical Reality in Noncovalent Interactions. *J. Mol. Model.* **2015**, *21* (3), 52. https://doi.org/10.1007/s00894-015-2585-5.

(26) Brinck, T.; Borrfors, A. N. Electrostatics and Polarization Determine the Strength of the Halogen Bond: A Red Card for Charge Transfer. *J. Mol. Model.* **2019**, *25* (5), 125. https://doi.org/10.1007/s00894-019-4014-7.

(27) Clark, T.; Murray, J. S.; Politzer, P. A Perspective on Quantum Mechanics and Chemical Concepts in Describing Noncovalent Interactions. *Phys. Chem. Chem. Phys.* **2018**, *20* (48), 30076–30082. https://doi.org/10.1039/C8CP06786D.

(28) Frenking, G.; Solà, M.; Vyboishchikov, S. F. Chemical Bonding in Transition Metal Carbene Complexes. *Journal of Organometallic Chemistry* **2005**, *690* (24–25), 6178–6204. https://doi.org/10.1016/j.jorganchem.2005.08.054.

(29) Bruce, Ê. D. V.; Rocha, W. R. Structure and Nature of the Metal–Ligand Interactions in Mixed Iron(II) Phosphametallocenes. *Organometallics* **2004**, *23* (22), 5308–5313. https://doi.org/10.1021/om0495473.

(30) Uddin, J.; Boehme, C.; Frenking, G. Nature of the Chemical Bond between a Transition Metal and a Group-13 Element: Structure and Bonding of Transition Metal Complexes with Terminal Group-13 Diyl Ligands ER (E = B to Tl; R = Cp, $N(SiH_3)_2$, Ph, Me). *Organometallics* **2000**, *19* (4), 571–582. https://doi.org/10.1021/om990936k.

(31) Varadwaj, P. R.; Varadwaj, A.; Marques, H. M. Halogen Bonding: A Halogen-Centered Noncovalent Interaction Yet to Be Understood. *Inorganics* **2019**, *7* (3), 40. https://doi.org/10.3390/inorganics7030040.

(32) Ang, S. J.; Mak, A. M.; Wong, M. W. Nature of Halogen Bonding Involving π-Systems, Nitroxide Radicals and Carbenes: A Highlight of the Importance of Charge Transfer. *Phys. Chem. Chem. Phys.* **2018**, *20* (41), 26463–26478. https://doi.org/10.1039/C8CP04075C.

(33) Kellett, C. W.; Kennepohl, P.; Berlinguette, C. P. π Covalency in the Halogen Bond. *Nature Commun.* **2020**, *11* (1), 3310. https://doi.org/10.1038/s41467-020-17122-7.

(34) Hamlin, T. A.; Bickelhaupt, F. M.; Fernández, I. The Pauli Repulsion-Lowering Concept in Catalysis. *Acc. Chem. Res.* **2021**, *54* (8), 1972–1981. https://doi.org/10.1021/acs.accounts.1c00016.

(35) Hamlin, T. A.; Fernández, I.; Bickelhaupt, F. M. How Dihalogens Catalyze Michael Addition Reactions. *Angew. Chem. Int. Ed.* **2019**, *58* (26), 8922–8926. https://doi.org/10.1002/anie.201903196.

(36) Hamlin, T. A.; Swart, M.; Bickelhaupt, F. M. Nucleophilic Substitution (S_N2): Dependence on Nucleophile, Leaving Group, Central Atom, Substituents, and Solvent. *ChemPhysChem* **2018**, *19* (11), 1315–1330. https://doi.org/10.1002/cphc.201701363.

(37) Stei, M.; Carrascosa, E.; Kainz, M. A.; Kelkar, A. H.; Meyer, J.; Szabó, I.; Czakó, G.; Wester, R. Influence of the Leaving Group on the Dynamics of a Gas-Phase SN2 Reaction. *Nat. Chem.* **2016**, *8* (2), 151–156. https://doi.org/10.1038/nchem.2400.

(38) Reed, A. E.; Weinstock, R. B.; Weinhold, F. Natural Population Analysis. *J. Chem. Phys.* **1985**, *83* (2), 735–746. https://doi.org/10.1063/1.449486.

(39) Mitoraj, M. P.; Michalak, A. σ-Donor and π-Acceptor Properties of Phosphorus Ligands: An Insight from the Natural Orbitals for Chemical Valence. *Inorg. Chem.* **2010**, *49* (2), 578–582. https://doi.org/10.1021/ic901736n.

(40) Kost, D.; Aviram, K. α-Substituent Effects and Non-Bonding Electron Interactions at the S_N2 Transition State, an ab-initio Study. *Tetrahedron Lett.* **1982**, *23* (40), 4157–4160. https://doi.org/10.1016/S0040-4039(00)88374-4.

(41) Dapprich, S.; Frenking, G. Investigation of Donor-Acceptor Interactions: A Charge Decomposition Analysis Using Fragment Molecular Orbitals. *J. Phys. Chem.* **1995**, *99* (23), 9352–9362. https://doi.org/10.1021/j100023a009.

(42) Xiao, M.; Lu, T. Generalized Charge Decomposition Analysis (GCDA) Method. *J. Adv. Phys. Chem.* **2015**, *04* (04), 111–124. https://doi.org/10.12677/JAPC.2015.44013.

(43) Gaussian 09, Revision D.01, M. J. Frisch, G. W. Trucks, H. B. Schlegel, G. E. Scuseria, M. A. Robb, J. R. Cheeseman, G. Scalmani, V. Barone, G. A. Petersson, H. Nakatsuji, X. Li, M. Caricato, A. Marenich, J. Bloino, B. G. Janesko, R. Gomperts, B. Mennucci, H. P. Hratchian, J. V. Ortiz, A. F. Izmaylov, J. L. Sonnenberg, D. Williams-Young, F. Ding, F. Lipparini, F. Egidi, J. Goings, B. Peng, A. Petrone, T. Henderson, D. Ranasinghe, V. G. Zakrzewski, J. Gao, N. Rega, G. Zheng, W. Liang, M. Hada, M. Ehara, K. Toyota, R. Fukuda, J. Hasegawa, M. Ishida, T. Nakajima, Y. Honda, O. Kitao, H. Nakai, T. Vreven, K. Throssell, J. A. Montgomery, Jr., J. E. Peralta, F. Ogliaro, M. Bearpark, J. J. Heyd, E. Brothers, K. N. Kudin, V. N. Staroverov, T. Keith, R. Kobayashi, J. Normand, K. Raghavachari, A. Rendell, J. C. Burant, S. S. Iyengar, J. Tomasi, M. Cossi, J. M. Millam, M. Klene, C. Adamo, R. Cammi, J. W. Ochterski, R. L. Martin, K. Morokuma, O. Farkas, J. B. Foresman, and D. J. Fox, Gaussian, Inc., Wallingford CT, 2016.

(44) *Schmidt, J.R.; Polik, W.F. WebMO Enterprise, Version 20.0; WebMO LLC: Holland, MI, USA, 2020.*

(45) Zhao, Y.; Truhlar, D. G. The M06 Suite of Density Functionals for Main Group Thermochemistry, Thermochemical Kinetics, Noncovalent Interactions, Excited States, and Transition Elements: Two New Functionals and Systematic Testing of Four M06-Class Functionals and 12 Other Functionals. *Theor. Chem. Acc.* **2008**, *120* (1–3), 215–241. https://doi.org/10.1007/s00214-007-0310-x.

(46) Cohen, A. J.; Mori-Sánchez, P.; Yang, W. Challenges for Density Functional Theory. *Chem. Rev.* **2012**, *112* (1), 289–320. https://doi.org/10.1021/cr200107z.

(47) Feller, D. The Role of Databases in Support of Computational Chemistry Calculations. *J. Comp. Chem.* **1996**, *17* (13), 1571–1586.

(48) Schuchardt, K. L.; Didier, B. T.; Elsethagen, T.; Sun, L.; Gurumoorthi, V.; Chase, J.; Li, J.; Windus, T. L. Basis Set Exchange: A Community Database for Computational Sciences. *J. Chem. Inf. Model.* **2007**, *47* (3), 1045–1052. https://doi.org/10.1021/ci600510j.

(49) Papajak, E.; Zheng, J.; Xu, X.; Leverentz, H. R.; Truhlar, D. G. Perspectives on Basis Sets Beautiful: Seasonal Plantings of Diffuse Basis Functions. *J. Chem. Theory Comput.* **2011**, *7* (10), 3027–3034. https://doi.org/10.1021/ct200106a.

(50) Ochterski, J. W. Thermochemistry in Gaussian. **2000**.

(51) Bernhard Schlegel, H. Estimating the Hessian for Gradient-Type Geometry Optimizations. *Theoret. Chim. Acta* **1984**, *66* (5), 333–340. https://doi.org/10.1007/BF00554788.

(52) Simons, J.; Joergensen, P.; Taylor, H.; Ozment, J. Walking on Potential Energy Surfaces. *J. Phys. Chem.* **1983**, *87* (15), 2745–2753. https://doi.org/10.1021/j100238a013.

(53) Banerjee, A.; Adams, N.; Simons, J.; Shepard, R. Search for Stationary Points on Surfaces. *J. Phys. Chem.* **1985**, *89* (1), 52–57. https://doi.org/10.1021/j100247a015.

(54) Baker, J. An Algorithm for the Location of Transition States. *J. Comput. Chem.* **1986**, *7* (4), 385–395. https://doi.org/10.1002/jcc.540070402.

(55) Baker, J. An Algorithm for Geometry Optimization without Analytical Gradients. *J. Comput. Chem.* **1987**, *8* (5), 563–574. https://doi.org/10.1002/jcc.540080502.

(56) Peng, C.; Bernhard Schlegel, H. Combining Synchronous Transit and Quasi-Newton Methods to Find Transition States. *Isr. J. Chem.* **1993**, *33* (4), 449–454. https://doi.org/10.1002/ijch.199300051.

(57) Lu, T.; Chen, F. Multiwfn: A Multifunctional Wavefunction Analyzer. *J. Comput. Chem.* **2012**, *33* (5), 580–592. https://doi.org/10.1002/jcc.22885.

(58) Humphrey, W.; Dalke, A.; Schulten, K. VMD: Visual Molecular Dynamics. *J. Mol. Graph.* **1996**, *14* (1), 33–38. https://doi.org/10.1016/0263-7855(96)00018-5.

(59) Persistence of Vision Pty. Ltd., Persistence of Vision Raytracer (Version 3.6), 2004, Http://Www.Povray.Org/Download/.

To format double-column figures, schemes, charts, and tables, use the following instructions:

Place the insertion point where you want to change the number of columns
From the **Insert** menu, choose **Break**
Under **Sections**, choose **Continuous**
Make sure the insertion point is in the new section. From the **Format** menu, choose **Columns**
In the **Number of Columns** box, type **1**
Choose the **OK** button

Now your page is set up so that figures, schemes, charts, and tables can span two columns. These must appear at the top of the page. Be sure to add another section break after the table and change it back to two columns with a spacing of 0.33 in.

Table 1. Example of a Double-Column Table

Column 1	Column 2	Column 3	Column 4	Column 5	Column 6	Column 7	Column 8

Authors are required to submit a graphic entry for the Table of Contents (TOC) that, in conjunction with the manuscript title, should give the reader a representative idea of one of the following: A key structure, reaction, equation, concept, or theorem, etc., that is discussed in the manuscript. Consult the journal's Instructions for Authors for TOC graphic specifications.

Insert Table of Contents artwork here